A dual-camera skylight polarisation imaging system supervised by an Ethernet network

Louise Ravolafidy, Charley Thom, Stéphane Viollet, Julien Serres

A dual-camera skylight polarisation imaging system supervised by an Ethernet network

Louise E Ravolafidy[1,2], Charley Thom[1,3], Stéphane Viollet[1] and Julien R Serres[1,4]

[1]Aix Marseille Univ, CNRS, ISM, Marseille, France

[2]Aix Marseille Univ, Polytech Marseille, GII, Marseille, France

[3]Institut d'Optique Graduate School, IOGS, Palaiseau, France

[4]Institut Universitaire de France, IUF, Paris, France

E-mail: julien.serres@univ-amu.fr

Abstract. Monitoring the state of polarisation of the skylight is valuable for polarisation-based embodied navigation systems, meteorology, atmospheric measurements, insects' behaviour, mobile robotics and remote sensing. This study presents the design and implementation of a dual-camera optical system capable of acquiring and processing polarized skylight images from a pair of cameras. The acquisition system integrates two complementary polarisation imaging strategies: Division of Time (DoT) and Division of Focal Plane (DoFP), allowing the real-time acquisition of high-res images and polarisation data. A complete hardware and software architecture was developed, including a Raspberry Pi-based control unit, a user-friendly graphical user interface (GUI), and dedicated acquisition workflows for each camera. Indoor experiments validate the system's ability to capture and visualize key polarisation parameters such as Degree of Linear polarisation (DoLP) and Angle of polarisation (AoP). AoP pattern can be either globally or locally computed, which is very useful for image processing. Although challenges remain in integrating both devices within a single software environment, the results demonstrate the potential of this system to collect polarisation data. Our setup offers a promising tool for long-term data recording, supporting future developments in numerous scientific fields including embodied intelligence in robotics.

Keywords. Polarized camera; Image processing; polarisation patterns detection; optical instrument; data acquisition.

1 Introduction

Polarisation patterns in the sky, caused by the scattering of sunlight in the atmosphere, carry rich and underused information. These patterns, invisible for the human eye, depend on the wavelength, time of day, weather conditions, and observer position. Insects like bees or ants are equipped with all the required sensors and circuitry embedded in their eyes and small brains to process the polarized skylight for navigation purposes for miles [1]. Measuring and modelling the polarised sky patterns can bring valuable insights to a wide range of fields, including atmospheric modelling [2–4], environmental monitoring [5–7], and navigation applications [8–11]. This study aims at developing an optical instrument equipped with polarisation-sensitive cameras to observe skylight over extended periods of time. The goal is to collect a large image database that will help the scientific community to better model the polarisation patterns of

the sky, considering variations across different wavelengths, positions, and weather conditions. A deeper understanding of these patterns is relevant for developing bio-inspired navigation systems, especially for autonomous vehicles operating in Global Navigation Satellite System (GNSS)-denied environments [8,11]. This technical study introduces the complete implementation of a dual-camera polarisation imaging system. In section 2, the state of the art in polarisation imaging is briefly presented. In section 3, we describe the hardware architecture, the Python-based acquisition software, and results from early experiments performed under controlled indoor conditions are presented in section 4. Next, a discussion about the embodiment of light polarisation detection on board robots is presented in section 5. Finally, a conclusion is drawn in section 6.

2 State of the art

Polarisation imaging has been the subject of increasing interest due to its ability to reveal information beyond standard intensity-based vision for navigation purposes [11–14]. This section reviews the key developments in the field and highlights the gaps that motivate our work to design and assemble an optical sky observation instrument to simultaneously detect the skylight polarisation pattern in both ultraviolet and visible wavelengths, which haven't been deeply investigated yet [4, 6, 9].

2.1 Light polarisation

We briefly recall the basic concepts of light polarisation, to clarify the parameters used in this article. Whenever light hits a linear polarizer, the angled vibrations are filtered out with only directed vibrations passing through (Fig. 1a). When light vibration is restricted to one plane, it is called linearly polarised. As it happens, light is said to be polarised when its electric field (at a fixed point in space) follows an elliptical motion over time. This elliptical movement can be described using two key parameters (Fig. 1b):

- The great axis azimuth a, which gives the orientation of the ellipse's main axis (Fig. 1b).
- The ellipticity angle e, which is the angle between the great axis azimuth a, and the diagonal of the smallest rectangle containing the ellipse. This angle is positive when the electric field rotates counterclockwise, and negative when it rotates clockwise around the direction of light propagation (Fig. 1b).

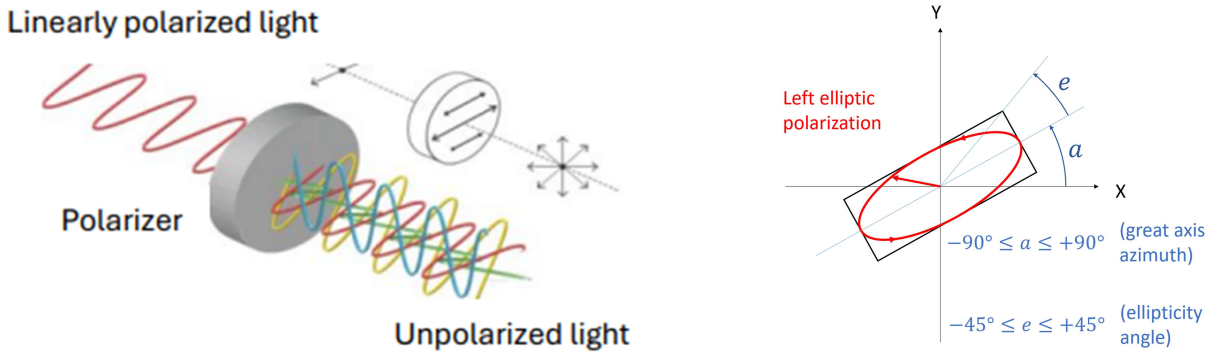

(a) (b)

Figure 1: polarisation formalism. (a) Example of linearly polarized light. (b) polarisation ellipse, where the z axis is the propagation axis (here it goes toward the reader). Adapted from [3].

2.2 Degree of Polarisation (DoP)

When the ellipticity a is zero (Fig. 1b), the polarisation is linear. This is typically the case in phenomena like atmospheric scattering due to the interactions between sun light and oxygen and nitrogen molecules in the atmosphere. Since the skylight can be partially polarised, we use a common measure called the Degree of Polarisation (DoP). The latter shows us how much light is polarised compared to the total amount of light. In other words, the DoP is the ratio between the polarised light intensity and the total

light intensity I_{total}. In our case, we only focus on the Degree of linear Polarisation (DoLP), because atmospheric scattering only emits linear polarisation [3].

2.3 Stokes formalism

To mathematically describe the polarisation state of light, we use the Stokes formalism [15]. The Stokes vector is composed of four components $S = [S_0, S_1, S_2, S_3]^T$. S_0 represents the total light intensity, S_1 and S_2 describe linear polarisation, S_3 (Fig. 2). These values are derived from the measured intensities of polarised light at different orientations (0°, 45°, 90°, 135°), as well as circular polarisation in clockwise and counterclockwise directions (or Left C_L, Right C_R) (1).

$$\begin{cases} S_0 \\ S_1 \\ S_2 \\ S_3 \end{cases} = \begin{cases} I_0 + I_{90} = I_{total} \\ I_0 - I_{90} \\ I_{45} - I_{135} \\ I_{C_L} + I_{C_R} \end{cases} \tag{1}$$

A useful way to visualize these components is the Poincaré sphere [16], where each point represents a specific polarisation state (Fig. 2). In natural outdoor lighting conditions, circular or elliptical polarisation is rarely present. Therefore, S_3 is considered to be null [11].

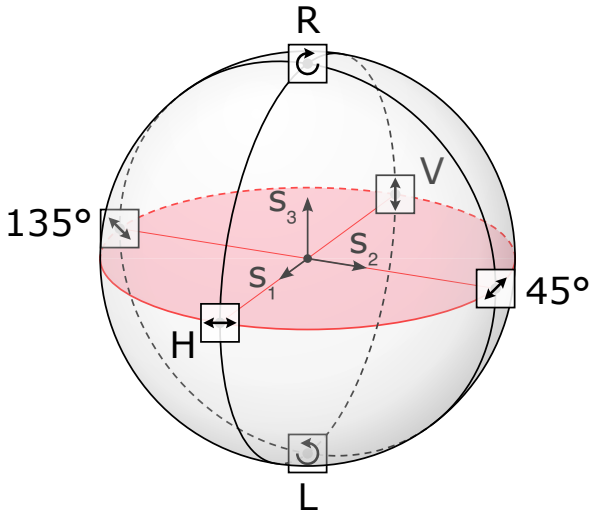

Figure 2: Poincaré sphere. In the equatorial plane (in pink), we can find purely linear polarisations that are also considered in our study. R: Right, L: Left, H: Horizontal, V: Vertical. Adapted from [11].

As Stokes vectors can be calculated from the intensities of light polarized at different angles, the DoLP can be determined by the same vectors (2).

$$DoLP = \frac{\sqrt{S_1^2 + S_2^2}}{S_0} \tag{2}$$

2.4 Angle of polarisation (AoP)

The polarisation direction is perpendicular to the scattering plane (Fig. 3). Therefore, from the observer's point of view, we can describe this direction using an orientation angle. This angle is called the Angle of Polarisation (AoP) and goes from 0° to 180° [5]. In this study, we use two types of AoP (Fig. 3):

- *AoPl*: the local AoP, which is the angle between the polarisation axis and the meridian plane of the particle (true vertical). This angle shows us where the light is coming from and has the same physical meaning as the azimuth angle a in Fig. 1b.
- *AoPg*: the global AoP, which is the angle between the polarisation axis and the observer reference direction. This angle illustrates how the polarisation axis is oriented on the image sensor, after the light has passed through the optics. As shown in Fig. 3, in the observer frame, α_p represents the azimuth for a random particle. The *AoPg* angle is defined through *AoPl* (3), and is given by:

$$AoPg = AoPl + \alpha_p \tag{3}$$

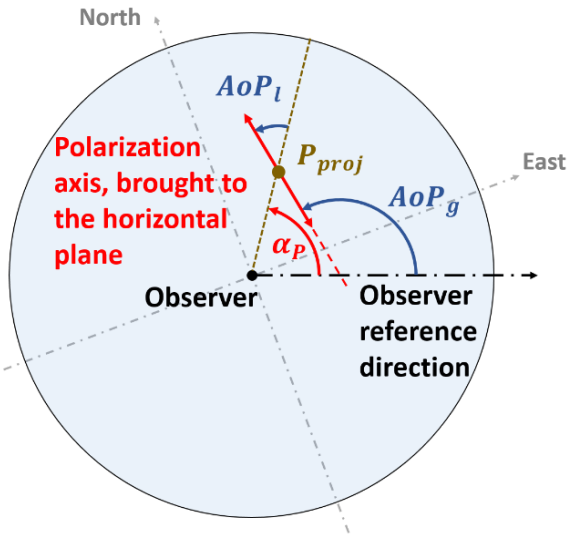

Figure 3: Definition of the local Angle of polarisation $AoPl$ and the global Angle of polarisation $AoPg$. Adapted from [3].

Like the DoP, $AoPg$ can also be determined by Stokes vectors (4).

$$AoPg = 0.5 \cdot arg(S_1 + i \cdot S_2) \tag{4}$$

2.5 Polarisation acquisition techniques

There are several techniques to acquire the intensity of light polarised at different angles required for estimating the Stokes vectors. The two most common approaches are Division of Time (DoT) and Division of Focal Plane (DoFP) imaging [11,17]. In this study, we use both techniques depending on the availability of imaging technologies.

2.5.1 Division of Time (DoT) DoT imaging consists of capturing multiple images sequentially at fixed timing intervals, each with a different polarisation analysis state. This is achieved by placing a Polarisation State Analyser (PSA) in front of the camera, which is shared by all pixels. The analyser is adjusted between acquisitions to perform the different measurements needed to estimate the Stokes vectors (Fig. 4a). The main advantage of this method is that each pixel captures all the required polarisation states, resulting in a full-resolution Stokes image, matching the native resolution of the sensor. However, it is highly sensitive to changes in the scene (like sun occlusion by clouds), since different acquisitions happen one after another.

2.5.2 Division of Focal Plane (DoFP) DoFP imaging, on the other hand, performs diverse polarisation measurements simultaneously using different pixels on the sensor (Fig. 4b). Each pixel is equipped with its own integrated polarisation filter, allowing all the necessary measurements to be captured in a single acquisition. This makes DoFP much less sensitive to scene motion or weather changing in our application, which is a clear advantage for embedded systems and real-time applications. However, this technique reduces spatial resolution because each polarisation state is derived from four neighbouring pixels. As a result, the final Stokes image has an effective resolution four times lower than the native resolution of the imager.

Although DoT offers full data but lacks real-time usability, and DoFP is faster but less precise, few studies have attempted to combine the strengths of both systems. No unified solution currently allows joint acquisition and supervision of both camera types in a single platform. That gap leads us to the central research questions of this work: can a unified software tool allow users to control both

devices, adjust acquisition parameters, and visualize complementary polarisation data (AoPs and DoLP patters) in real time from ultraviolet range to visible range? To explore this question, we designed and implemented a combined hardware-software architecture.

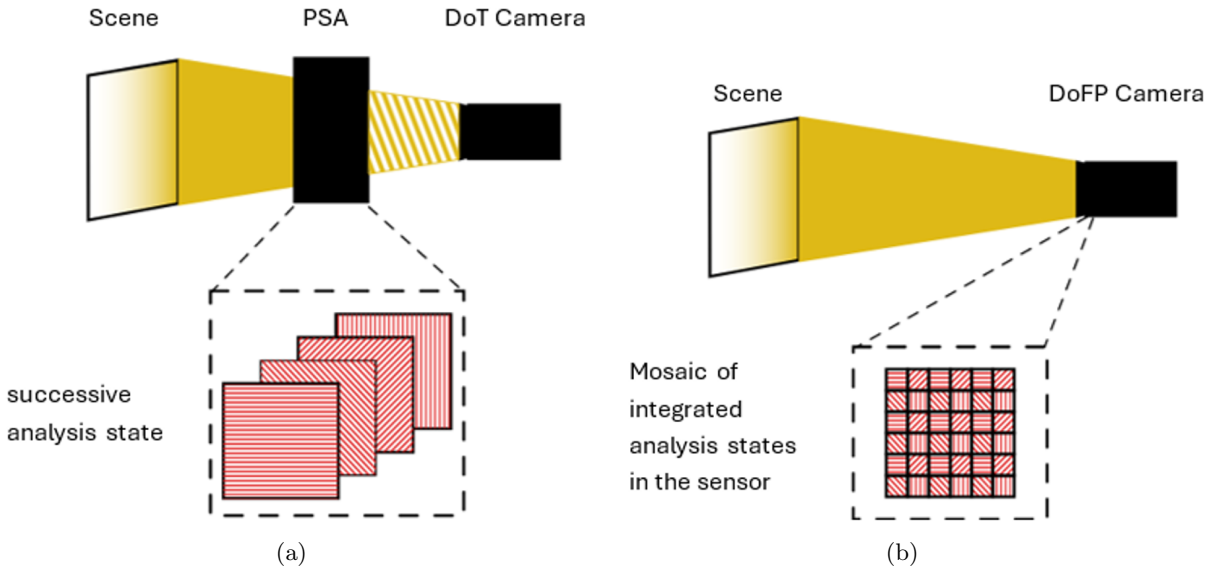

Figure 4: Acquisition techniques. (a) Illustration of Division of Time (DoT) camera including the polarisation state analiyzer (PSA). The successive analysis states represented correspond to linear polarisation measurements at different orientations, shown here for simplicity. (b) Illustration of Division of Focal Plane (DoFP) camera. The sensor's mosaic of integrated analysis also corresponds to linear polarisation filters oriented in various directions. From [17].

3 Materials and Methods

Based on the limitations identified in the literature and taking into account the availability of commercial imagers on the market [11], we developed a dual-camera system combining these two complementary acquisition techniques. This section presents the methods used to collect and process polarisation data from both ultraviolet and visible ranges.

3.1 Hardware architecture

We designed a complete hardware architecture for our optical sky observation instrument. It is structured into three main functional blocks commonly found in automated systems: the Operational Part, the Control Unit, and the Human-Machine Interface shown in Fig. 6.

3.2 Operational Part

This section includes all physical elements that interact with the external environment.

3.2.1 DoT acquisition technique Our study focused on the design and development of a system implementing the principles of the DoT acquisition technique (see section 2.5.1). The acquisition system is composed of an ultraviolet (UV)-sensitive camera GOX-8105M-PGE (JAI group, Copenhagen, Denmark), equipped with a UV lens fl-bc2528-vguv (Ricoh Ltd., Tokyo, Japan) (Fig. 5a). As PSA, a piezoelectric motor, the ELL14K (Thorlabs, Inc., Newton, New Jersey, United States), is used to rotate both a UV linear polarizing filter LPUV100 (Thorlabs, Inc., Newton, New Jersey, United States) and a UV-pass filter FGUV5 (Thorlabs, Inc., Newton, New Jersey, United States), both mounted directly on the motor (Fig. 5a). Connection between these components is described in Fig. 6. This setup allows polarisation filtering to be modulated in time by rotating polarising filters placed in front of the camera lens. With this method, we obtain four polarised images (0°, 90°, 45°, and 135°). None of the parameters listed above are given by the camera. Therefore, these images need to be treated before having an estimation of AoPs and DoLP patterns.

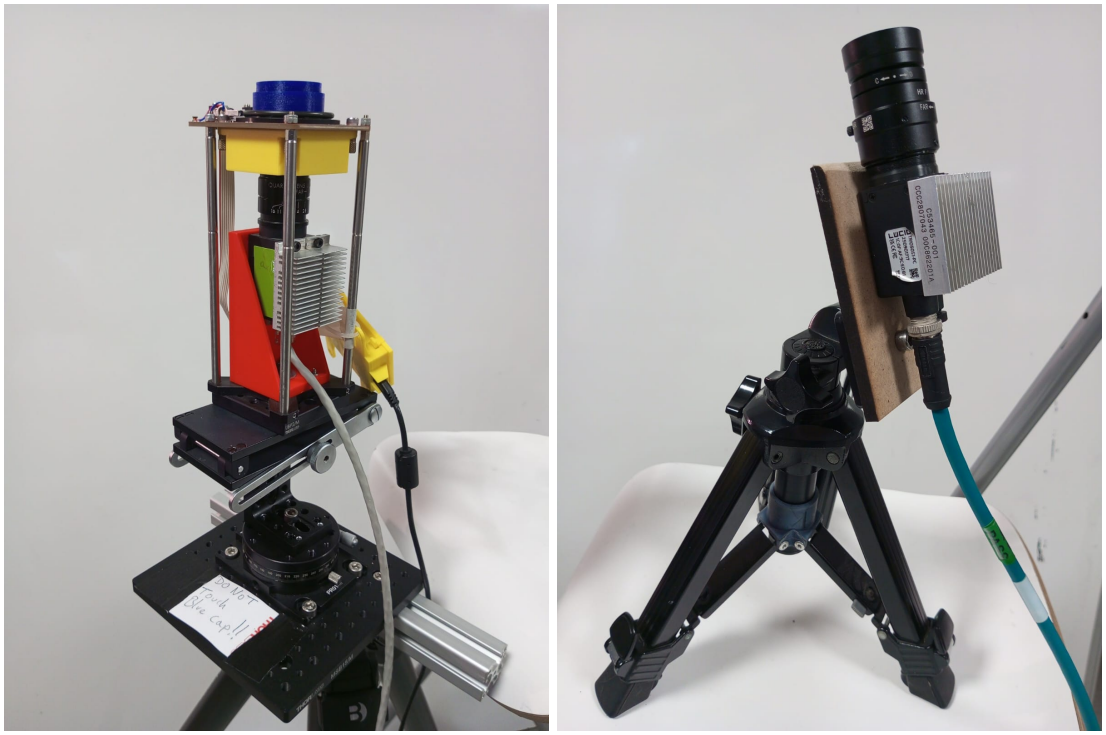

(a) (b)

Figure 5: (a) Ultraviolet (UV)-sensitive camera GOX-8105M-PGE equipped with a UV lens fl-bc2528-vguv and covered with a rotating polarised filter. (b) Triton polarisation camera TRI050S1-P with Sony's IMX264MZR/MYR polarised CMOS mono sensors, and a high resolution lens HR F1.2/6mm

3.2.2 DoFP acquisition technique We used the Triton polarisation camera TRI050S1-P with Sony's IMX264MZR/MYR polarized CMOS mono sensors (LUCID Vision Lab, Richmond, BC, Canada), and a high-res lens HR F1.2/6mm (Edmund Optics, Barrington, New Jersey, United States) (Fig. 5b). Connections between these components are described in Fig. 6.

This kind of sensor is designed to easily compute the first three Stokes parameters (S_1, S_2, S_3) and is polarised with four different directional polarising filters (0°, 90°, 45°, and 135°). The imagers also allow the acquisition of four simultaneous polarisation angles at the pixel level (see section 2.5.2). In terms of parameters, *DoLP* and *AoPg* patterns are given by the camera; the *AoPl* angle is deducted from the *AoPg* angle (3). These two cameras are complementary for sky imaging: the GOX-8105M-PGE camera is sensitive to UV light (Fig. 7a), while the TRI050S1-P camera operates in the visible spectrum (Fig. 7b). Since UV radiation is invisible to the human eye, the visible-sensitive camera also serves as a reference to verify and compare the results obtained from the UV-sensitive camera.

3.2.3 Power over Ethernet (PoE) Switch The PoE Switch (Fig. 6) acts as the central hub for both power and network data transfer between the cameras and the Raspberry Pi board. We use the DEXLAN 4GE (PSE) + 1 GE PD input PoE repeater model (DEXLAN, Mantes-en-Yvelines, France) - GE: Gigabit Ethernet, PSE: Power Sourcing Equipment, PD: Powered Device.

3.2.4 Control Unit The central processing (Fig. 6) is handled by a Raspberry Pi 4 model B (Raspberry Pi Foundation, Cambridge, United Kingdom), which plays a crucial role in the system : it drives all system components through our developed Python-based code using Software Development Kits (SDKs) of eaxh camera; it also handles data acquisition, pre-processing (frame conversion, saving images, etc.), and communication with the user interface.

3.2.5 Human-Machine Interface (HMI) This interface allows the user to interact with the system in real-time. The HMI allows to show live cameras, parameter controls, and image previews (e.g., AoPs,

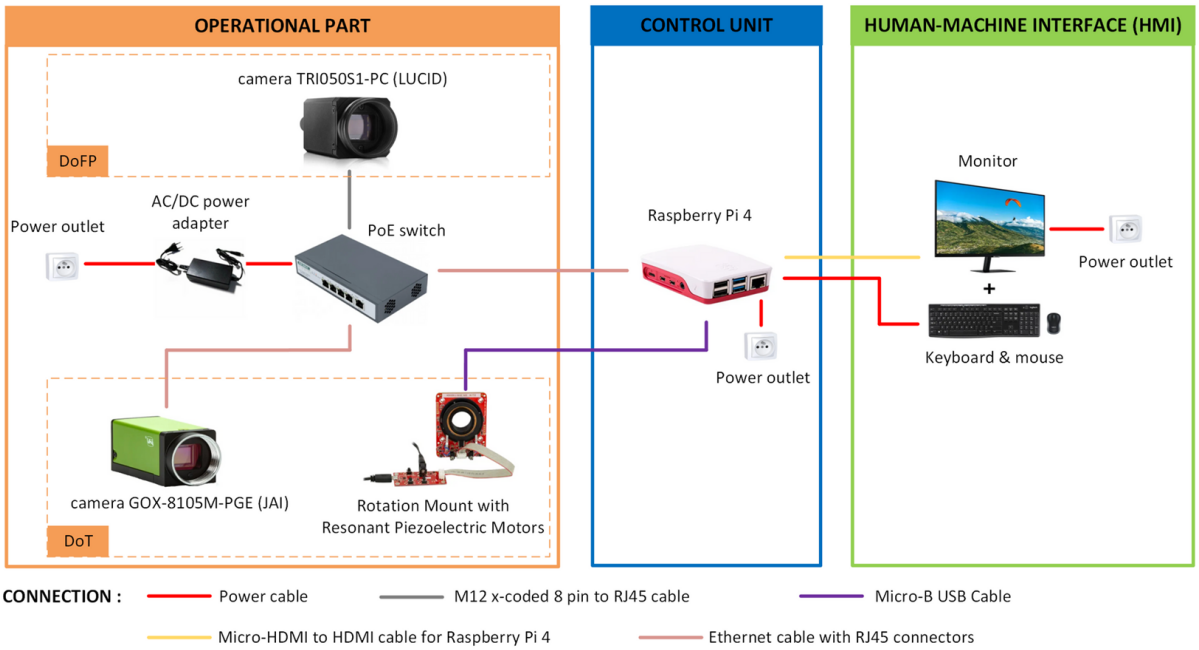

Figure 6: Schematic representation of the full hardware setup of the developed system. DoFP stands for Division of Focal Plane, DoT stands for Division of Time, AC/DC means Alternative Current / Direct Current, PoE represents Power over Ethernet.

DoLP visualisations), a keyboard and mouse that enable the user to navigate through the GUI, configure acquisition parameters, and trigger image capture (Fig. 6). This functional block is essential for manual control, debugging, and monitoring the system.

3.3 Software architecture

The following flowchart (Fig. 8) illustrates the overall software architecture designed to control both polarisation cameras, manage data acquisition, and supervise user interactions.

The process in Fig. 8 begins with a network check between the Raspberry and the connected cameras. If the connection fails, the user is prompted to configure the Internet Protocol (IP) addresses and subnet masks to ensure proper communication over Ethernet between them. Once the connection is established, the main supervision interface can be launched, allowing the user to select between the two imaging devices. For the DoFP acquisition system, the user can do four main actions:

- Configure the camera: Adjust the gain and exposure time to optimise the acquisition conditions. On the one hand, gain refers to the amplification of the electrical signal generated by the photosensors when it captures light, measured in decibels. On the other hand, exposure time is the amount of time the imager is exposed to incoming light from the scene, measured in microseconds.
- Stream camera view: Display a real-time video feed sent by the camera. This feature allows the user to visually confirm the effects of gain and exposure adjustments; and most importantly, to physically align the cameras with a specific point in the sky before acquisition.
- Acquire a single image (Format Mono8): Capture one frame corresponding to the selected output mode: DoLP, AoPG, AoPL, or raw intensity image. This feature enables the user to perform a quick capture, visualise the result immediately, and save the output image in .png format.
- Acquire multiple images (Format Mono12 & Mono8): Launch a sequence of image acquisitions based on user-defined parameters. The user specifies the total duration, the time interval between captures, and the destination folder. For each cycle, the system records a raw image and saves the corresponding AoPG, AoPL, and DoLP data as numerical matrices with the camera configurations. This function is suited for time series analysis or monitoring changes in polarisation patterns over time.

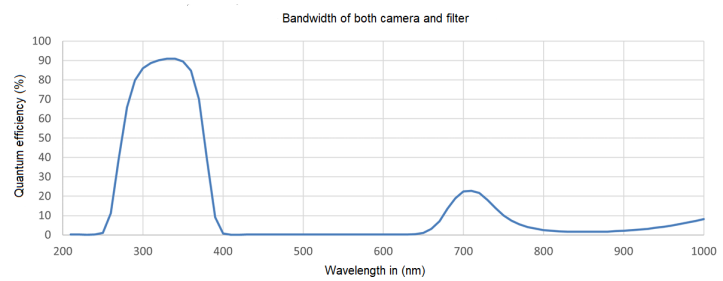

(a)

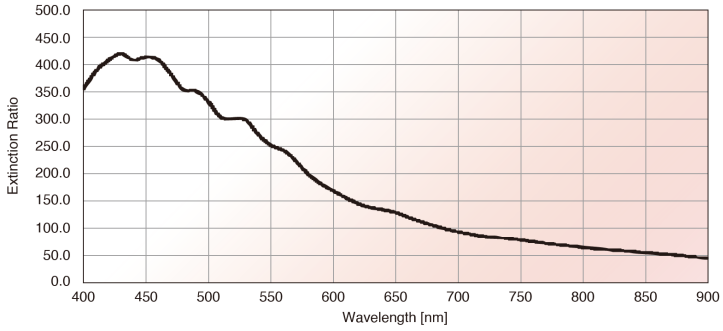

(b)

Figure 7: (a) Spectral response of the ultraviolet (UV)-sensitive camera GOX-8105M-PGE fitted with a UV lens fl-bc2528-vguv and covered with a rotating polarised filter. (b) Spectral response of the Triton polarisation camera TRI050S1-P fitted with Sony's IMX264MZR/MYR polarized (from technical documentation).

The DoT acquisition system (camera + motor) is triggered when the user selects the camera GOX-8105M-PGE. The software sends sequential commands to the piezoelectric motor to rotate the polarising filter to fixed angles: 0°, 45°, 90°, and 135°. After each rotation, the system waits for stabilisation, then captures a frame using the UV-sensitive camera and saves it in .tiff format. This process is repeated automatically for all four angles. The resulting set of images can be used for other patterns computation (DoLP, AoPs).

4 Results

This section presents the main results obtained with the dual-camera polarisation imaging system, followed by a discussion of their implications and limitations. Images (Fig. 9 only shows results from the visible-sensitive camera) were acquired indoors, independently using a Raspberry Pi 4, with separate acquisition workflow for each camera. On the one hand, the DoFP camera was used to capture raw intensity, DoP, AoPG, and derived AoPL images of a calibration target. On the other hand, the DoT camera was tested to capture a sequence of polarised images at angles of 0°, 35°, 90°, and 135°. These initial results validate the ability of our control unit to handle both systems independently and confirm the relevance of the software tools developed.

While both cameras were successfully integrated and operated independently on Windows 10 Pro and Raspberry Pi 4 operating systems. Two integration acquisition techniques were tested to manage the dual-camera setup. In the first approach, the user selects which camera to use before launching an acquisition, using a dedicated camera selection interface. In the second approach, both cameras are handled within a unified graphical user interface (GUI) (Fig. 10), where camera-specific controls are dynamically activated based on the selection. We also tested identifying the cameras based on their respective IP addresses.

Moreover, a feature to convert .tiff images into a matrix form should be integrated into the program. Indeed, by processing matrices, it becomes possible to compute the Stokes vector (1), from which we can estimate the DoP and AoPs patterns.

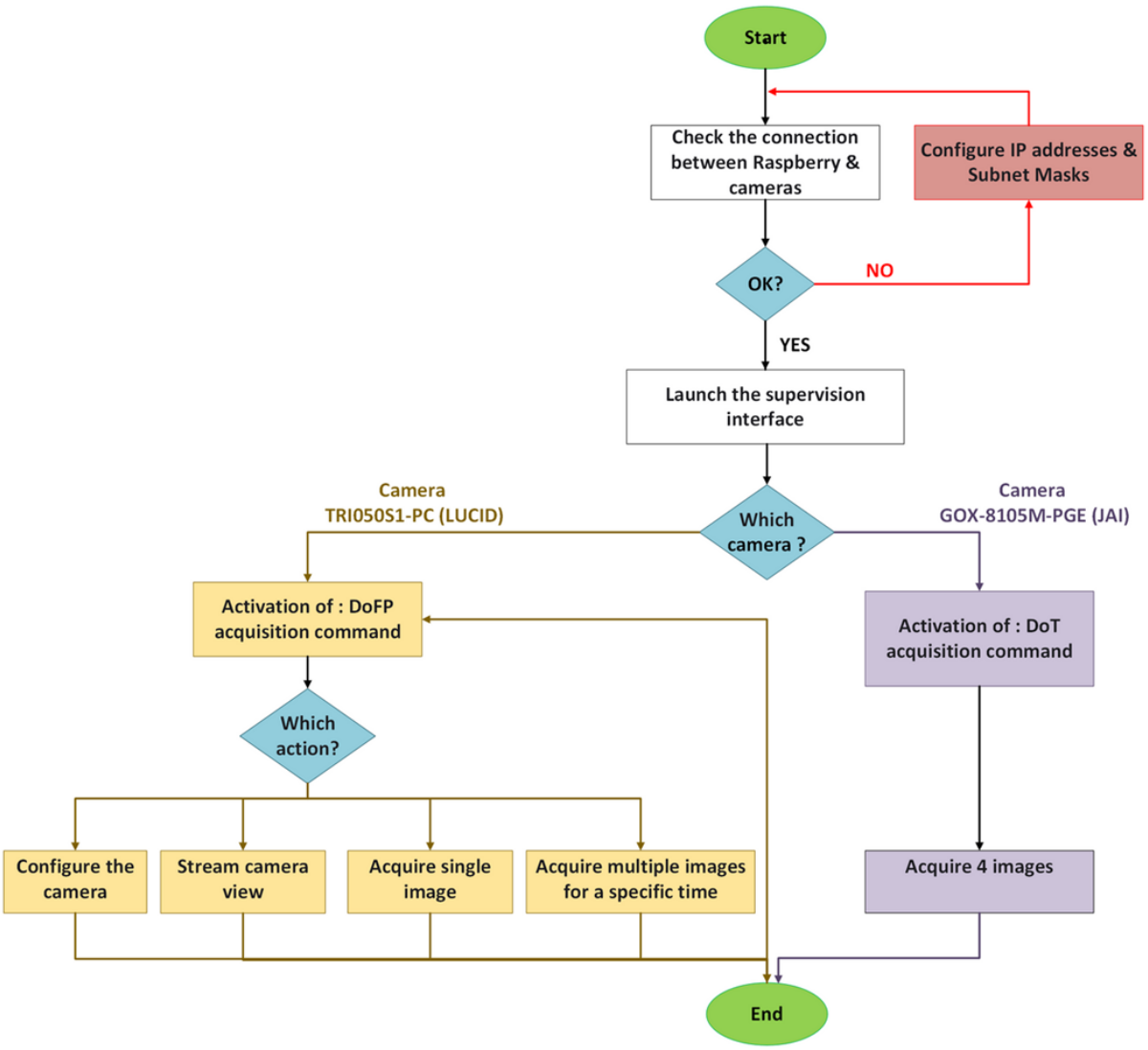

Figure 8: Software architecture flowchart of the developed supervision interface. IP means Internet Protocol, DoFP stands for Division of Focal Plane, DoT stands for Division of Time, *DoLP* means Degree of Linear Polarisation, *AoPg* represents the global Angle of Polarisation, and *AoPl* stands for local Angle of Polarisation.

5 Discussion about the embodiment of light polarisation detection on board robots

5.1 Embodiment in polarisation-based sensory modality

The skylight polarisation pattern consists of E-vectors distributed along concentric circles around the Sun (Fig. 11a). The degree of polarisation in the sky gradually increases up to a maximum of about 0.75 along a circle located 90° from the Sun (Fig. 11a).

When the Sun is not directly visible for various reasons (obstruction, limited field of view, clouds, etc.), it has been clearly demonstrated [19] that a bee or an ant sensitive to polarised skylight can estimate the Sun's position (azimuth and elevation) by processing the polarisation patterns (DoP and AoPs patterns) using photoreceptors equipped with polarisation filters (microvilli) located in the dorsal rim area (DRA) of the compound eye (Figs. 11b-d).

In each ommatidium of the DRA, the microvilli of photoreceptor cell 7 are oriented perpendicularly to those of photoreceptors 1, 2, 5, 6, and 8 (inset in Fig. 11b). The microvilli of photoreceptors 3 and 4 are irregularly arranged (inset in Fig. 11b).

As suggested by Thomas Labhart in his model inspired by the polarisation-processing units (POL

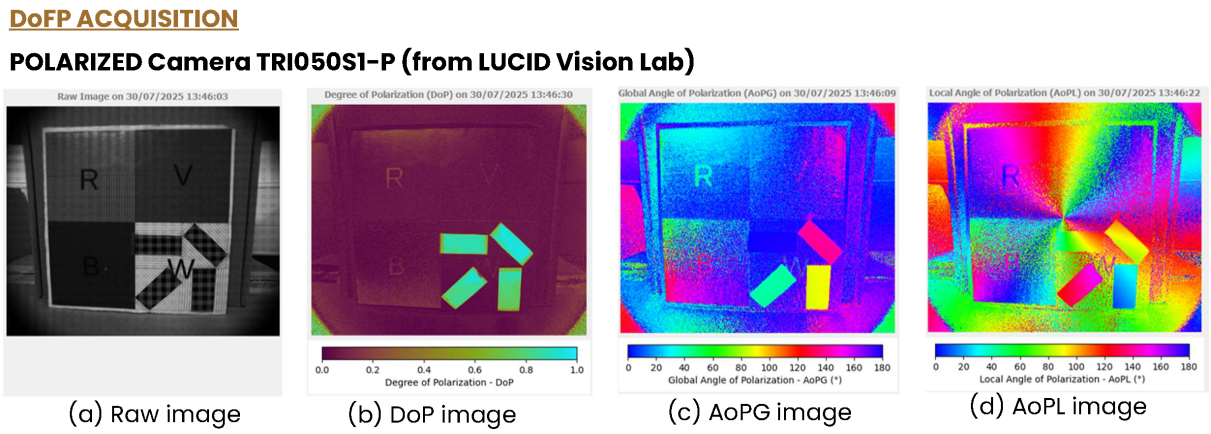

Figure 9: Calibration pattern with four polarized filters (0°, 45°, 90°, 135°) at the bottom right. The images were captured by the "Acquire a single image (Mono 8)" mode with the TRI050S1-P camera during an indoor test at the lab. (a) Raw image directly captured by the camera. (b) Degree of polarisation (DoP) image computed directly by the camera. (c) Global Angle of polarisation (AoPG) image obtained from the built-in processing. (d) Local Angle of polarisation (AoPL) image estimated from the AoPG. The point at the center of the image corresponds to the optical center of the camera, as determined by the calibration toolbox [18].

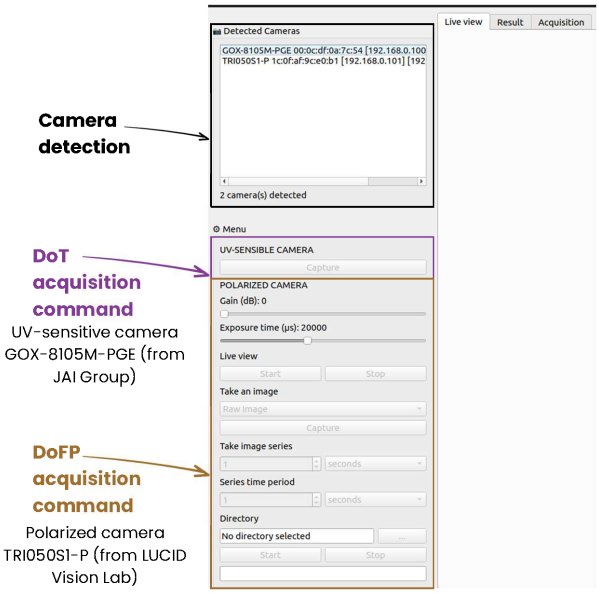

Figure 10: Unified interface design where camera-specific buttons and sliders are dynamically enabled depending on the selected device.

neurons) found in the locust [20], a POL neuron efficiently computes the log-ratio of the outputs of two photoreceptors equipped with orthogonally oriented polarisation filters.

The AoP and DoP can be computed using an analog logarithmic amplifier and by orienting several POL neurons according to different preferred directions. This is precisely the case in the cricket, whose POL neurons have three preferred polarisation orientations corresponding to maximum intensity. It has been shown that three orientations are sufficient to reconstruct the Stokes parameters with an excellent signal-to-noise ratio [21]. Nevertheless, for technological simplicity, four orientations (0°, 45°, 90°, and 135°) are typically used in polarimetric cameras featuring division of focal plane configuration.

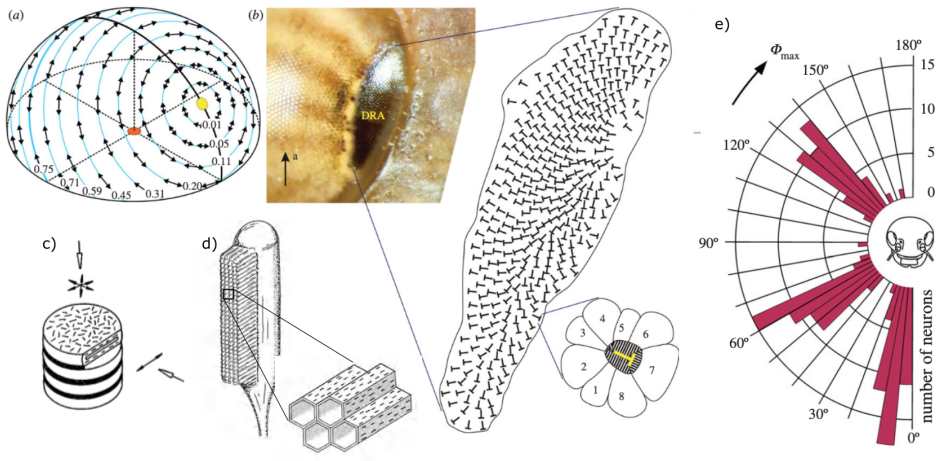

Figure 11: Polarised vision in the desert locust *Schistocerca gregaria* as an example of smart embodiment. (a) Pattern of polarised skylight. The electric field vectors (e-vectors, double arrows) are arranged along concentric circles around the Sun (yellow). Direct sunlight is not polarised. (b) Dorsal Rim Area (DRA) sensitive to polarisation in the left compound eye of a locust, illustrating the arrangement of the ommatidia and the structure of a DRA ommatidium. (c) The chromophores are randomly distributed within a photoreceptor, whereas they are aligned in the lateral part of the tube (d). (e) Histogram of e-vector tunings from 142 recordings from POL1 neurons. Three physiological types can be distinguished with maximum orientations around 10°, 60° and 130° with respect to the longitudinal axis of the animal. Adapted from [22].

5.2 Polarisation-based embodied navigation systems

Most of works on skylight polarisation detection has been mainly investigated in the visible range in order to detect the heading angle, which can be either the angle with the solar meridian or the geographic North Pole, in clear sky conditions to test their accuracy [11]. Research achievements are often verified with captured sunny sky images databases [7, 23] or simulated sky images databases [3, 24–26].

However, models based on deep neural networks trained and validated on simulated datasets do not reach the required level of accuracy for their applications in field robotics. For instance, a ResNet-18 model reached a median absolute error of 1.0° on simulated datasets with cloud masks, and 4.3° on the captured sky images databases [27]. In the study [28], a U-Net model was trained with a simulated sky images database to isolate the radial invariance from a temporal series of DoLP patterns. After removing outliers, the authors obtained a mean absolute error of 1.6° (9.0° with outliers) [28].

Consequently, simulated or clear sky images databases do not reflect the real skylight imperfections that occur, especially with the presence of heavily overcast skies, in order to conveniently train deep neural networks. That's why, jointly recordings of sky images database in the visible and UV ranges by means of our dual-camera skylight polarisation imaging system will be helpful to generate databases whatever the cloud coverage. The detection of the skylight polarisation pattern in the UV range will be particularly relevant because it is less sensitive to the cloud coverage [29–31].

6 Conclusion

In this technical study, we designed a dual-camera system for detecting the skylight polarisation patterns combining two complementary approaches to capture the skylight polarisation pattern: a Division of Time (DoT)-based camera to detect it in the ultraviolet (UV) range and a Division of Focal Plane (DoFP)-based camera to detect it in the visible range. As far we know, DoFP-based cameras working in the UV range haven't been designed and marketed yet. This dual-camera system was integrated into a compact hardware architecture using a Raspberry Pi 4 and a Power over Ethernet (PoE) network, supported by a dedicated graphical user interface (GUI) written in Python language.

The proposed solution was validated through a series of test acquisitions using separately both cameras. The DoFP acquisition offered real-time access to polarisation data such as DoLP and AoP patterns; while the DoT acquisition enabled high-res acquisition through sequential rotations of a polarising filter. Together, our dual-camera acquisition system provides a complete and complementary view of skylight

polarisation states from UV range to visible range in order to better model polarisation patterns whatever the wavelength or to estimate atmosphere optical properties, or to better understand insects' behaviour by coupling it with the skylight polarisation, as well as to generate images database to train AI-based algorithms for polarisation-based embodied navigation systems.

It remains some limitations in this work-in-progress study: for example, long acquisitions over any weather conditions haven't been done yet. Our dual-camera polarisation imaging system works on Windows 10 Pro and Raspberry Pi 4 operating systems. The architecture and tools developed in this study lay a solid foundation for future improvements. We made these recent developments completely open to the scientific community. Moving forward, the objective is to deploy our acquisition system in outdoor conditions to record a long-term annotated database of sky polarisation images as already recorded over two months in the visible range in this data paper published in 2024 [7]. By linking each image with contextual information such as time, location, weather and so on, this dataset will support more accurate modelling of the skylight polarisation pattern or atmospheric measurements, as well as the development of polarisation-based algorithms for polarisation-based embodied navigation systems.

Data Availability Statement
Documentation and Python-based acquisition software of our dual-camera polarisation imaging system:
GitHub: https://github.com/elenahravolafidy/POLAR_Project

OpenSky polarisation pattern simulator code under CC-BY licence from [3]:
GitHub: https://github.com/MoutenetA/OpenSky
OSF: https://osf.io/rynv7/?view_only=13674c69c28148879f96dd472db11e2e

A two month-long annotated skylight polarisation images database in the visible range from [7]:
GitHub: https://github.com/mol-1/A-2-month-long-annotated-skylight-polarisation-images-databaseassociated-code
Recherche Data Gouv: https://entrepot.recherche.data.gouv.fr/dataset.xhtml?persistentId=doi:10.57745/9L2YUB

Funding
J.R.S. and S.V. were supported by Aix Marseille University and the CNRS Institutes (Biology, Informatics as well as Engineering). This work and the L.E.R. and C.T.'s internships were supported by the ANR ASTRID ECOPOL project, grant ANR-24-ASTR-0011 of the French Agence Nationale de la Recherche.

Acknowledgements
"Laboratoire d'Optique Atmosphérique (LOA, UMR 8518, CNRS/Université de Lille)" is acknowledged for helping us with the various tests carried out on our polarised cameras. We thank Jean-Marc Ingargiola for giving us the required tools and equipment to create the hardware part of our imaging system, and we also thank Camille Pléau, Antoine Moutenet, and Alexandre Dupont for helping us in designing our acquisition device.

References
[1] Rüdiger Wehner. *Desert navigator: the journey of an ant*. Harvard University Press, 2020.

[2] Thomas Kronland-Martinet, Léo Poughon, Marcel Pasquinelli, David Duché, Julien R Serres, and Stéphane Viollet. Skypole: a geolocation algorithm based on polarized vision without using astronomical ephemerides. In *Polarization: Measurement, Analysis, and Remote Sensing XVI*, volume 13050, pages 74–79. SPIE, 2024.

[3] Antoine Moutenet, Léo Poughon, Bruno Toulon, Julien R Serres, and Stéphane Viollet. Opensky: a modular and open-source simulator of sky polarization measurements. *IEEE Transactions on Instrumentation and Measurement*, 73:1–16, 2024.

[4] Clarissa M DeLeon and Meredith Kupinski. Ground-based ultraviolet polarimetry for imaging the babinet polarization neutral point. *Optical Review*, pages 1–9, 2025.

[5] Laura M Eshelman and Joseph A Shaw. Visualization of all-sky polarization images referenced in the instrument, scattering, and solar principal planes. *Optical Engineering*, 58(8):082418–082418, 2019.

[6] Léo Poughon, Vincent Aubry, Jocelyn Monnoyer, Stéphane Viollet, and Julien R Serres. A standalone polarimetric acquisition system for producing a long-term skylight dataset. In *2023 IEEE SENSORS*, pages 1–4. IEEE, 2023.

[7] Léo Poughon, Vincent Aubry, Jocelyn Monnoyer, Stéphane Viollet, and Julien R Serres. An extended database of annotated skylight polarization images covering a period of two months. *BMC Research Notes*, 17(1):306, 2024.

[8] Qingyun Zhang, Jian Yang, Panpan Huang, Xin Liu, Shanpeng Wang, and Lei Guo. Bionic integrated positioning mechanism based on bioinspired polarization compass and inertial navigation system. *Sensors*, 21(4):1055, 2021.

[9] Antoine Moutenet, Julien R Serres, and Stéphane Viollet. Ultraviolet vs. visible skylight polarization measurements. In *2023 IEEE SENSORS*, pages 01–04. IEEE, 2023.

[10] Yuyang Li, Xia Wang, Min Zhang, and Chao Xu. Ultraviolet bionic compass method based on non-ideality correction and statistical guidance in twilight conditions. *Optics Express*, 32(13):22132–22152, 2024.

[11] Julien R Serres, Pierre-Jean Lapray, Stéphane Viollet, Thomas Kronland-Martinet, Antoine Moutenet, Olivier Morel, and Laurent Bigué. Passive polarized vision for autonomous vehicles: a review. *Sensors*, 24(11):3312, 2024.

[12] Julien Dupeyroux, Stéphane Viollet, and Julien R Serres. Polarized skylight-based heading measurements: a bio-inspired approach. *Journal of the Royal Society Interface*, 16(150):20180878, 2019.

[13] Fang Kong, Yingjing Guo, Xiaojing Fan, Xiaohan Guo, et al. Review on bio-inspired polarized skylight navigation. *Chinese Journal of Aeronautics*, 36(9):14–37, 2023.

[14] Mingzhi Chen, Yuan Liu, Daqi Zhu, Wen Pang, and Jianmin Zhu. Underwater polarized light navigation: Current progress, key challenges, and future perspectives. *Robotics*, 14(8):104, 2025.

[15] George Gabriel Stokes. On the composition and resolution of streams of polarized light from different sources. *Transactions of the Cambridge Philosophical Society*, 9:399, 1851.

[16] Henri Poincaré. *Cours de physique mathématique: leçons sur la théorie mathématique de la lumière, professées pendant le premier semestre, 1887-1888*. Carré, 1889.

[17] Benjamin Le Teurnier. *Imagerie polarimétrique basée sur un capteur à micro-grilles: caractérisation et détection des erreurs dues aux fluctuations spatiales*. PhD thesis, Université Paris-Saclay, 2022.

[18] Davide Scaramuzza, Agostino Martinelli, and Roland Siegwart. A toolbox for easily calibrating omnidirectional cameras. In *2006 IEEE/RSJ International Conference on Intelligent Robots and Systems*, pages 5695–5701. IEEE, 2006.

[19] Samuel Rossel. Polarization sensitivity in compound eyes. In *Facets of vision*, pages 298–316. Springer, 1989.

[20] Thomas Labhart. Can invertebrates see the e-vector of polarization as a separate modality of light? *Journal of Experimental Biology*, 219(24):3844–3856, 12 2016.

[21] François Goudail and Arnaud Bénière. Estimation precision of the degree of linear polarization and of the angle of polarization in the presence of different sources of noise. *Applied optics*, 49(4):683–693, 2010.

[22] Uwe Homberg, Stanley Heinze, Keram Pfeiffer, Michiyo Kinoshita, and Basil El Jundi. Central neural coding of sky polarization in insects. *Philosophical Transactions of the Royal Society B: Biological Sciences*, 366(1565):680–687, 2011.

[23] Huaju Liang, Hongyang Bai, Ke Hu, and Xinbo Lv. Bioinspired polarized skylight orientation determination artificial neural network. *Journal of Bionic Engineering*, 20(3):1141–1152, 2023.

[24] Huaju Liang, Hongyang Bai, Ning Liu, and Kai Shen. Limitation of rayleigh sky model for bioinspired polarized skylight navigation in three-dimensional attitude determination. *Bioinspiration & Biomimetics*, 15(4):046007, 2020.

[25] Huaju Liang and Hongyang Bai. Polarized skylight navigation simulation (psns) dataset. *arXiv preprint arXiv:2007.13081*, 2020.

[26] Xin Wang, Jun Gao, and Nicholas William Roberts. Bio-inspired orientation using the polarization pattern in the sky based on artificial neural networks. *Optics Express*, 27(10):13681–13693, 2019.

[27] L Yadala Chanchu, RFG Zuidgeest, DM Stam, and GCHE de Croon. Robust heading estimation from polarization images by deep neural networks. In *International Micro Air Vehicle Conference*, pages 56–63, 2024.

[28] Thomas Kronland-Martinet, Léo Poughon, Antoine Moutenet, Marcel Pasquinelli, David Duché, Julien R Serres, and Stéphane Viollet. Locating the north celestial pole from skylight polarization patterns and solar declination. *IEEE Transactions on Instrumentation and Measurement*, 2025.

[29] András Barta and Gábor Horváth. Why is it advantageous for animals to detect celestial polarization in the ultraviolet? skylight polarization under clouds and canopies is strongest in the uv. *Journal of Theoretical Biology*, 226(4):429–437, 2004.

[30] Xin Wang, Jun Gao, and Zhiguo Fan. Empirical corroboration of an earlier theoretical resolution to the uv paradox of insect polarized skylight orientation. *Naturwissenschaften*, 101(2):95–103, 2014.

[31] Xiangwei Zeng, Yan Zhang, Xueye Chen, and Xindong Sun. Transmission characteristics of linearly polarized light in altostratus help explain "uv-sky-pol" paradox. *Optica Applicata*, 54(2):129–134, 2024.